Melt mixing causes negative correlation of trace element enrichment and CO_2 content prior to an Icelandic eruption

Supplementary material

David A. Neave, John Maclennan, Marie Edmonds, Thorvaldur Thordarson

A Analytical methods and VSD calculation methods

A.1 Secondary ion mass spectrometry (SIMS)

All SIMS analyses were performed on a Cameca ims-4f instrument at the NERC Ion Microprobe Facility at the University of Edinburgh, UK across two analytical sessions in November 2012 and April 2013.

Carbon (C) was measured separately from other volatiles and trace elements. When measuring C, the SIMS configured with a high mass resolving power in order to ensure good separation of ^{12}C and $^{24}Mg^{2+}$ peaks. Other volatiles and trace elements were subsequently measured in a second round of analyses. SIMS measurements of C were the first measurements made on the samples: samples were C-coated and analysed by EPMA after SIMS to prevent the risk of contamination from the C-coat. Measurements were made using a primary O^- ion beam with an accelerating voltage of 15 kV, a beam current of 5 nA, a secondary accelerating voltage of 4500 V minus a 50 V offset and a 25 μm image field. The ion beam was rastered over an area of approximately 25 μm^2 for >120 s prior to analysis to remove surface contamination. The raster was then switched off and a 10 μm beam centred in the middle of the rastered area was used to make measurements. The following isotopes were measured for 20 cycles, with counting times in seconds in parentheses: $^{12}C(5)$, $^{24}Mg^{2+}(10)$, $^{28}Si^{2+}(2)$ and $^{30}Si(2)$. Only counts from the final 10 cycles, when count rates reach an asymptote and the effects of surface contamination are minimal, were retained to calculate C concentrations. A background correction was performed by subtracting the number of C counts measured using the CO_2-free standard N-72 (Shishkina et al., 2010) and fully CO_2 degassed matrix glasses samples. C concentrations were calculated using a calibration curve constructed with a suite of basaltic glass standards of CO_2 content 0–2000 ppm prepared by Isobel R. Sides using samples from Hauri et al. (2002) and Shishkina et al. (2010). Average accuracy was estimated as ±0.1% by comparison of measured concentrations with published compositions determined by FTIR. Precision was estimated as 1σ = ±5% using 12 repeat analyses of both standards and samples.

Water (H_2O), fluorine (F) and trace elements were measured as part of the same analysis set-up after C analyses had been completed. Measurements were made using a primary O^- ion beam with an accelerating voltage of 15 kV, a beam current of 5 nA, a secondary accelerating voltage of 4500 V minus a 75 V offset and a 25 μm image field. Analyses were made with a spot size of approximately 25μm x 25μm centred in the pit made during the preceding C analysis. The following isotopes were measured for 20 cycles, with counting times in seconds in parentheses: $^{1}H(5)$, $^{19}F(5)$, $^{30}Si(2)$, $^{35}Cl(5)$, $^{39}K(3)$, $^{47}Ti(3)$, $^{84}Sr(3)$, $^{85}Rb(3)$, $^{88}Sr(3)$, $^{89}Y(3)$, $^{90}Zr(3)$, $^{93}Nb(3)$, atomic mass 130.5(3), $^{138}Ba(3)$, $^{139}La(3)$, $^{140}Ce(3)$, $^{141}Pr(5)$, $^{143}Nd(5)$, $^{149}Sm(8)$, $^{151}Eu(10)$, $^{156}Gd(5)$, $^{159}Tb(10)$, $^{161}Dy(10)$, $^{165}Ho(10)$, $^{167}Er(15)$, $^{169}Tm(20)$, $^{171}Yb(20)$, $^{174}Yb(20)$, $^{175}Lu(20)$ and $^{178}Hf(20)$. Peak positions were verified before each analysis, and mass 130.5 was measured to determine backgrounds in each cycle, which were always sufficiently close to zero to be ignored. H_2O concentrations were calculated using a calibration curve constructed with M10 and M40 glass standards with H_2O contents of 0.75 and 3.07 wt.% respectively prepared by Isobel R. Sides using samples from Shishkina et al. (2010). Accuracy was estimated at ±10% based on the comparison of measured M10 and M40 compositions with published values. Precision was estimated as 1σ = ±10% using 15 repeat analyses of M10 and M40. Drift was monitored using repeat analyses of M10 and M40 at the start, middle and end of each day. 9% drift in calculated H_2O concentrations was observed on two days of H_2O data collection and a linear correction was made. F concentrations were calculated using a calibration curve constructed with the international standards GSD-1G, ML3B-G and BCR-2G (Jochum et al., 2005, 2006). Accuracy was estimated at ±30% based on the

comparison of measured GSD-1G, ML3B-G and BCR-2G compositions with published values (Jochum et al., 2005, 2006). Precision was estimated as $1\sigma = \pm 5\%$ using 15 repeat analyses of M10 and M40.

NIST-610 was used as the calibration standard for trace element analyses (e.g. Jochum et al., 2011). Concentrations were calculated by normalising ^{30}Si to Si determined subsequently by EMPA at the University of Cambridge. The following international standards were measured at the start of each day to monitor the calibration and drift: GSD-1G, BCR-2G, GOR132-G, ML3B-G (Jochum et al., 2005, 2006). The trace element content of M10 and M40 was also monitored throughout each day to check for drift, though none was observed. Absolute element concentrations were calculated using JCION-6 software, where corrections were also made for oxide interferences of light REEs on the heavy REEs and BaO on Eu. The magnitude of oxide correction relates to the offset voltage at which the data are processed. The appropriate offset voltage varied between different samples, and was found to be 77±5 V. The second analytical session was normalised to the first using the mean composition of ML3B-G from each session, which was the most measured standard in both sessions.

Accuracy was monitored by analysis of international standards, ML3B-G, GOR128-G and BCR-2G throughout analytical sessions. Using ML3B-G, which has the most similar composition to the measured samples, accuracy was estimated at ±5% or better for all trace elements apart from Lu (-11%). Using GOR128-G, accuracy was estimated at ±10% or better for most trace elements except Rb (200%), La (72%), Nd (−20%), Sm (13%), Dy (−18%) and Hf (21%). However, GOR128-G is highly depleted, and consequently highly incompatible elements have concentrations at or below the detection limit of SIMS. Poor estimates of accuracy from this sample are therefore not indicative of poor analyses of real samples. Using BCR2-G, accuracy was estimated at ±8% or better for all trace elements apart from Nd (−10%), Sm (21%) and Tm (−15%). Precision was estimated as $1\sigma = \pm 5\%$ using 15 repeat analyses of M10 and M40 for trace elements of high abundance (e.g. Ce, Sr) and as up to $1\sigma = \pm 10\%$ for trace elements of low abundance (e.g. Lu, Hf).

A.2 Electron probe microanalysis (EPMA)

Major element compositions of macrocrysts, matrix glasses and melt inclusions were determined using a Cameca SX100 instrument at the University of Cambridge, UK. Glass analyses were performed with a spot size of 10 μm, an operating potential of 15 kV and a beam current of 6 nA. Macrocryst analyses were performed with an operating potential of 15 kV and a beam current of 10 nA. Counting times were as follows: 20 s for major elements in glass and macrocrysts except for Ti which was counted for 60 s and Na which was counted for 10 s; 30 s for trace elements in crystals; 60 s for P, Cr, Mn and Ni in glass. Calibration standards were as follows: jadeite for Na, periclase for Mg, Si glass for Si, K-feldspar for K, rutile for Ti, fayalite for Fe, corundum for Al, apatite for P, and pure metals for Cr, Mn and Ni. Data reduction was performed using the inbuilt Cameca X-Phi PeakSight software for glass analyses and PAP corrections for mineral analyses. Most analyses returned totals of 98.5–100.5 wt.%. Samples with totals outside this range or with inappropriate stoichiometry were discarded. Forsterite content of the St. John's Island Olivine standard was determined with a precision of $\pm 0.46 (2\sigma)$ mol.% (n=27).

A.3 Vesicle size distribution (VSD) calculation

Vesicles were traced digitally on high-resolution (3600 dpi) scans of two thin sections from Skuggafjöll. Vesicle areas were then measured using the analyse particle tool in ImageJ (http://rsb.info.nih.gov/ij/), enabling vesicle diameters (L) to be calculated for further analysis. A stereological correction factor of 1.18 was applied to vesicle diameters by assuming that all vesicles are perfect spheres (Cashman and Marsh, 1988; Mangan et al., 1993). Vesicles were divided into 100 μm size bins and plotted on VSD diagrams of L versus $\ln(n)$. Vesicle number densities (N_t) were calculated from regression lines fitted through linear sections VSD diagrams. In both cases the smallest size bins (<0.1 mm) was discarded from regressions because small vesicles were not reliably traced, leading to the underestimation of population densities. Large size bins (>1 mm) were also discarded from regressions because they do not contain statistically meaningful vesicle populations. Additionally, large vesicles may have either experienced coalescence or have been inherited from previous vesiculation events.

B Supplementary figure

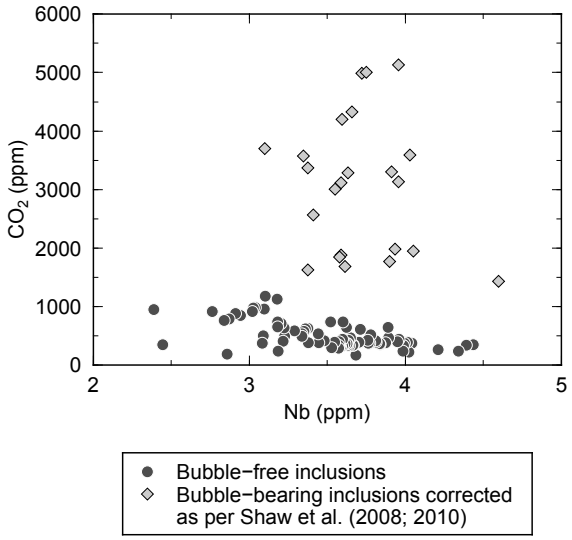

Fig. B.1: Plot comparing the CO_2 content of bubble-free melt inclusions with the CO_2 content of bubble-bearing melt inclusions corrected using the method of Shaw et al. (2008, 2010). Inclusion-hosted bubbles are assumed to be in equilibrium with the glass portion of melt inclusion, enabling a CO_2 content to be calculated using the ideal gas law. By applying the correction all bubble-bearing inclusions have CO_2 contents above the range defined by bubble-free inclusions. Calculated inclusion-hosted bubble CO_2 densities of 0.24-0.82 g/cm^3 are well above the detection limit of CO_2 by Raman spectroscopy. The correction method of Shaw et al. (2008, 2010) is therefore inapplicable in the case of Skuggafjöll, indicating that bubbles are not in equilibrium with glassy portions of melt inclusions.

References

Cashman, K.V., Marsh, B.D., 1988. Crystal size distribution (CSD) in rocks and the kinetics and dynamics of crystallization. 2. Makaopuhi lava lake. Contributions to Mineralogy and Petrology 99, 277–291.

Hauri, E.H., Wang, J., Dixon, J.E., King, P.L., 2002. SIMS analysis of volatiles in silicate glasses: 1. calibration, matrix effects and comparisons with FTIR. Chemical Geology 183, 99–114.

Jochum, K.P., Stoll, B., Herwig, K., Willbold, M., Hofmann, A.W., Amini, M., Aarburg, S., Abouchami, W., Hellebrand, E., Mocek, B., Raczek, I., Stracke, A., Alard, O., Bouman, C., Becker, S., Dücking, M., Brätz, H., Klemd, R., de Bruin, D., Canil, D., Cornell, D., de Hoog, C.J., Dalpé, C., Danyushevsky, L., Eisenhauer, A., Gao, Y., Snow, J.E., Groschopf, N., Günther, D., Latkoczy, C., Guillong, M., Hauri, E.H., Höfer, H.E., Lahaye, Y., Horz, K., Jacob, D.E., Kasemann, S.A., Kent, A.J.R., Ludwig, T., Zack, T., Mason, P.R.D., Meixner, A., Rosner, M., Misawa, K., Nash, B.P., Pfänder, J., Premo, W.R., Sun, W.D., Tiepolo, M., Vannucci, R., Vennemann, T., Wayne, D., Woodhead, J.D., 2006. MPI-DING reference glasses for in situ microanalysis: New reference values for element concentrations and isotope ratios. Geochemistry Geophysics Geosystems 7, Q02008.

Jochum, K.P., Weis, U., Stoll, B., Kuzmin, D., Yang, Q., Raczek, I., Jacob, D.E., Stracke, A., Birbaum, K., Frick, D.a., Günther, D., Enzweiler, J., 2011. Determination of Reference Values for NIST SRM 610-617 Glasses Following ISO Guidelines. Geostandards and Geoanalytical Research 35, 397–429.

Jochum, K.P., Willbold, M., Raczek, I., Stoll, B., Herwig, K., 2005. Chemical Characterisation of the USGS Reference Glasses and BIR-1G Using EPMA , ID-TIMS , ID-ICP-MS and LA-ICP-MS. Geostandards and Geoanalytical Research 29, 285–302.

Mangan, M.T., Cashman, K.V., Newman, S., US Geological Survey, Hawaiian Volcano Observatory, 1993. Vesiculation of basaltic magma during eruption. Geology 21, 157–160.

Shaw, A.M., Behn, M.D., Humphris, S.E., Sohn, R.A., Gregg, P.M., 2010. Deep pooling of low degree melts and volatile fluxes at the 85°E segment of the Gakkel Ridge: Evidence from olivine-hosted melt inclusions and glasses. Earth and Planetary Science Letters 289, 311–322.

Shaw, A.M., Hauri, E.H., Fischer, T.P., Hilton, D.R., Kelley, K.A., 2008. Hydrogen isotopes in Mariana arc melt inclusions: Implications for subduction dehydration and the deep-Earth water cycle. Earth and Planetary Science Letters 275, 138–145.

Shishkina, T.A., Botcharnikov, R.E., Holtz, F., Almeev, R.R., Portnyagin, M.V., 2010. Solubility of H_2O- and CO_2-bearing fluids in tholeiitic basalts at pressures up to 500MPa. Chemical Geology 277, 115–125.